Quantitative Analysis of Oxidation State in Cerium Oxide Nanomaterials

Christopher M. Sims, Russell A. Maier, Aaron C. Johnston-Peck, Justin M. Gorham, Vincent A. Hackley, and Bryant C. Nelson

Material Measurement Laboratory, National Institute of Standards and Technology, 100 Bureau Drive, Gaithersburg, MD 20899, USA

ABSTRACT

Cerium oxide nanoparticles (nanoceria) are receiving increased attention from the research community due to the large number and wide range of their current and potential applications. The attractiveness of nanoceria for these various applications is rooted in their unique chemical properties, most prominent of which is their ability to alternate between the Ce^{3+} and Ce^{4+} oxidation states. While many analytical techniques and methods have been used to characterize the amounts of Ce^{3+} and Ce^{4+} present (Ce^{3+}/Ce^{4+} ratio) within nanoceria materials, very few studies have utilized multiple complementary analytical tools (orthogonal analysis) with technique-independent oxidation state controls for quantitative determinations of the Ce^{3+}/Ce^{4+} ratio. Use of technique-independent control samples should improve the comparison of oxidation state measurements across a wide range of analytical techniques. Here, we utilize electron energy loss spectroscopy (EELS) and X-ray photoelectron spectroscopy (XPS) to orthogonally characterize the oxidation states of a suite of commercially available nanoceria materials using technique-independent Ce^{3+} and Ce^{4+} controls. Similarities and differences between analytical results are discussed in the context of the products analyzed.

Keywords: ceria nanoparticles, characterization, oxidation state, orthogonal analysis

1. INTRODUCTION

Of the many engineered nanomaterials being incorporated into our society, cerium oxide nanoparticles (nanoceria) are receiving increased attention due to their current and potential use in a wide variety of applications.[1] While the performance of nanoceria in these applications depends on many factors, the ability of nanoceria to cycle between the Ce^{3+} and Ce^{4+} oxidation states has been proposed as the primary feature behind their unique abilities.[2] As such, accurate determination of the Ce^{3+}/Ce^{4+} ratio can significantly improve our understanding of nanoceria properties and interactions across a breadth of fields.

In the literature, several analytical techniques have been used to gain insight into the Ce^{3+}/Ce^{4+} ratios of nanoceria (e.g. electron energy loss spectroscopy (EELS), X-ray photoelectron spectroscopy (XPS), Raman spectroscopy), yet each of these techniques operates under different fundamental principles, and hence, are subject to producing different results depending on the technique utilized.[3] However, few studies have used multiple complementary analytical techniques, herein described as orthogonal analysis, for determining the Ce^{3+}/Ce^{4+} ratios in nanoceria analytes. Even in the few cases where orthogonal analysis was performed, technique-independent control samples of known oxidation state were not utilized,[4-5] which further complicates comparison of experimental results between individual analytical techniques.

Here, we describe the development of an analytical procedure designed to measure the cerium oxidation state in nanoceria using orthogonal approaches. Preparation of materials for control measurements and methods for optimizing data acquisition and processing were developed to efficiently analyze and objectively interpret the distribution of Ce^{3+} vs. Ce^{4+} oxides using EELS and XPS. The methodology is applied to quantify the Ce^{3+}/Ce^{4+} ratios in commercially available nanoceria materials.

2. MATERIALS AND METHODS[1]

2.1 Materials

Complete details of materials used and synthesis methods are described elsewhere.[6] Bulk cerium (IV) oxide (CeO_2, 99.995% Ce) was purchased from Strem Chemicals, Inc. (Newburyport, MA). Cerium carbonate hydrate ($Ce_2(CO_3)_3 \cdot xH_2O$, 99.999%) and germanium oxide (GeO_2, 99.999%) were purchased from Alfa-Aesar (Haverhill, MA). Aluminum oxide (Al_2O_3, 99.99%) was purchased from Johnson and Matthey (Royston, UK). 2% Ge-doped $CeAlO_3$ (Ge-$CeAlO_3$) was prepared from Al_2O_3, $Ce_2(CO_3)_3 \cdot xH_2O$ and GeO_2 using traditional mixed oxide synthesis techniques modified from previously used methods.[7] Two commercially available nanoceria materials were obtained: a nanopowder comprised of vendor specified 25 nm primary particles (NPCO) and a fuel borne catalyst for diesel (FBC). All materials were used as received without further purification.

NIST Disclaimer: [1]Certain trade names and company products are mentioned in the text or identified in illustrations in order to adequately specify the experimental procedure and equipment used. In no case does such identification imply recommendation or endorsement by National Institute of Standards and Technology, nor does it imply that the products are necessarily the best available for the purpose.

2.2 Scanning Transmission Electron Microscopy (STEM) Imaging and Electron Energy Loss Spectroscopy (EELS)

High-angle annular dark field images and EELS data were collected using a probe-corrected FEI (Hillsboro, OR) Titan transmission electron microscope. The instrument was operated at 300 kV with a 25 pA beam current. For EELS acquisition the convergence and collection semi-angles were approximately 3.6 and 13.7 mrad, respectively. The dispersion was 0.05 eV/ch, and the FWHM of the zero-loss peak was 0.70 eV ± 0.05 eV. During the spectral acquisition the beam was rastered over an area of 0.026 μm^2, this was repeated in 6 or 7 different locations on the sample grid. To ensure a precise energy-loss scale, a custom Digital Micrograph script switched the drift tube excitation between the zero-loss region and the core-loss region as a series of spectra were recorded. In post-processing spectra were then aligned relative to the zero-loss peak and summed together.

Ge-$CeAlO_3$ and bulk CeO_2 were used as controls to provide the characteristic Ce^{3+} and Ce^{4+} spectra. A GSL least squares fit, as employed in EELSMODEL,[8] of the control spectra to the commercial samples was used for quantification of the EELS data. Backgrounds were removed and Fourier-ratio deconvolution routines applied to all spectra prior to fitting. More specific details of the EELS analysis can be found elsewhere.[6]

2.3 X-ray Photoelectron Spectroscopy (XPS)

Ge-$CeAlO_3$ and bulk CeO_2 were used as controls to generate representative spectra for Ce^{3+} and Ce^{4+}, respectively. The commercial nanoceria materials were analyzed in the form they were sold in, specifically as a powder pressed into copper tape (NPCO sample) or a drop cast suspension onto silicon wafer (FBC sample).

XP spectra were acquired on an Axis Ultra DLD XPS system from Kratos Analytical (Chestnut Ridge, NY) which was maintained at ultra-high vacuum (UHV) conditions, which was a base pressure of 2 x 10-9 torr. Spectra were generated using monochromated Al Kα X-rays to achieve photoemission of core level electrons which were acquired along the sample surface normal with 90% of the photoelectrons were collected over a 0.94 mm x 2.25 mm area as determined in previous studies.[9] Due to the insulating nature of the various cerium oxide materials, the surface of the samples were neutralized using low energy electrons to compensate for surface charging. Spectra were acquired at 160 eV pass energy with a step size of 1.0 eV for the wide survey spectra and at 40 eV pass energy with a step size of 0.1 eV for the higher resolution elemental regions.

The acquired spectra were processed using CasaXPS, a commercially available software. All spectra were energy corrected by shifting the C(1s) peak maximum binding energy (BE) to 284.6 eV. All Ce 3d spectra were fit with U2 Tougaard background with the second parameter in the cross-section field adjusted so the background intersected the noise between the Ce 3d5/2 and Ce 3d3/2 shakedown features for the Ce^{3+} spectra and between the Ce 3d5/2 and Ce 3d3/2 shakeup features for the Ce^{4+} spectra.[10] Semi-quantitative assessment of the distribution of ceria's oxidation states was based on the control sample's spectral lineshapes which were assumed to have 100% of their relative oxidation state. More specific details of the XPS analysis can be found elsewhere.[6]

3. RESULTS

3.1 Orthogonal Analysis of the NPCO Sample

A representative STEM image of the particles from the NPCO sample is shown in Figure 1. The average particle size, as determined from analysis of STEM images, was found to be 20.9 ± 12.5 nm (n = 300).

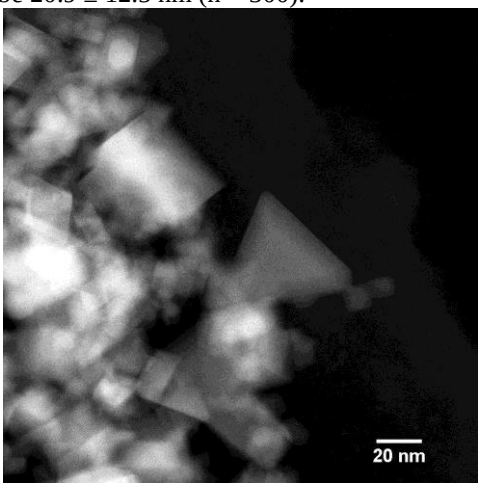

Figure 1. Representative STEM image of the NPCO sample. Scale bar: 20 nm.

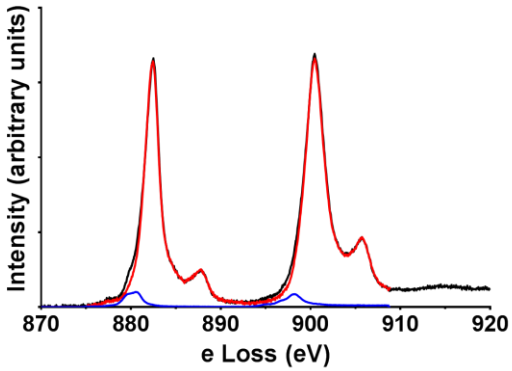

Figure 2. EEL spectra of the NPCO sample. Sample spectrum is shown in black, with contributions to the sample spectra from Ce^{4+} shown in red and contributions from Ce^{3+} shown in blue.

A Ce $M_{4,5}$ EEL spectrum for the NPCO sample is shown in Figure 2. The M edge excitations are due to electron transitions between 3d and 4f states. The 4f state of a Ce^{4+} ion is unoccupied while a Ce^{3+} ion has a single electron. These differences of occupancy are reflected in the electron

loss near edge structure (ELNES) of the EEL spectra. The Ce $M_{4,5}$ edges associated with Ce^{3+}, when compared to edges associated with Ce^{4+}, are shifted to lower energies, have different relative peak intensities, as well as different edge shapes (e.g., note the loss of the satellite peaks). In the NPCO sample, the Ce^{4+} contribution dominates most of the spectrum.

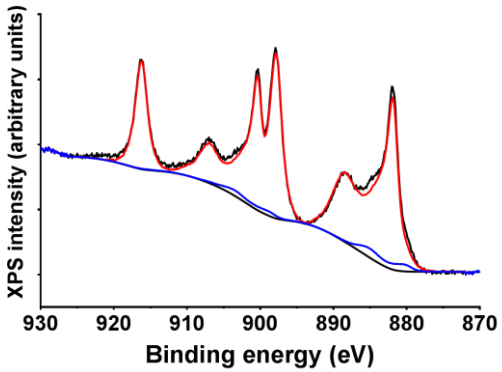

Figure 3. XP spectra of NPCO sample. The sample spectrum is shown in black, with contributions to the sample spectra from Ce^{4+} shown in red and contributions from Ce^{3+} shown in blue.

An XP spectrum of the Ce 3d region of the NPCO sample is shown in Figure 3. Contributions from Ce^{4+}, with the characteristic 6 peaks (two photoelectron peaks, each with a "shake-up" and "shake-down" satallite) dominate the spectrum. Contributions from Ce^{3+}, which consists of 4 peaks (two photoelectron peaks and two peaks from final state effects), comprise very little of the sample spectrum.

3.2 Orthogonal Analysis of the FBC Sample

A representative STEM image of the particles from the FBC sample is shown in Figure 4. The average particle size, as determined from analysis of STEM images, was found to be 4.9 ± 1.3 nm (n = 300).

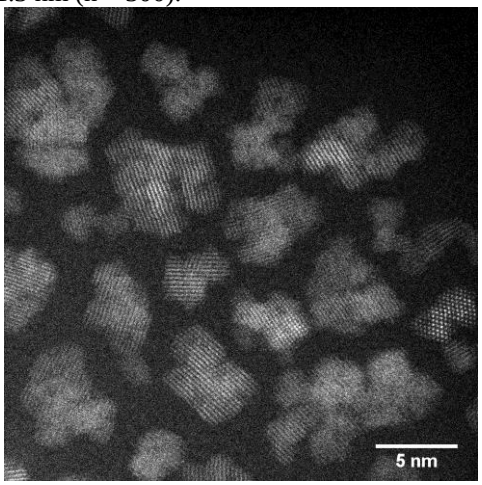

Figure 4. Representative STEM image of the FBC sample. Scale bar = 5 nm.

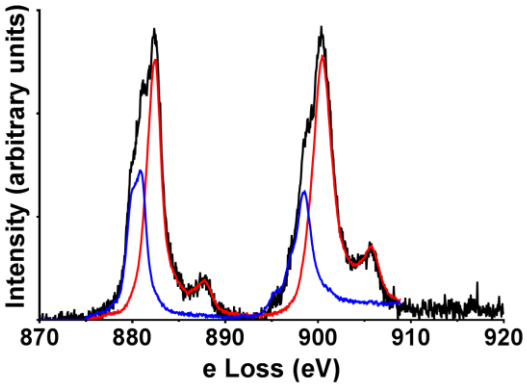

Figure 5. EEL spectra of the FBC sample. Sample spectrum is shown in black, with contributions to the sample spectra from Ce^{4+} shown in red and contributions from Ce^{3+} shown in blue.

A Ce $M_{4,5}$ EEL spectrum for the FBC sample is shown in Figure 5. Ce^{3+} and Ce^{4+} contributions to the spectra are as described in Section 3.1. Note the increased Ce^{3+} contribution in the FBC sample relative to the NPCO sample.

An XP spectrum of the Ce 3d region of the FBC sample is shown in Figure 6. Contributions from Ce^{4+} and Ce^{3+} are as described in Section 3.2. Note the lack of Ce^{3+} contribution to the XP spectrum.

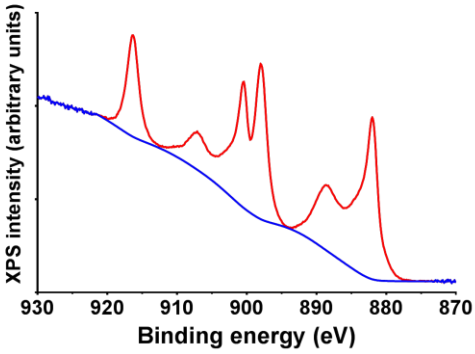

Figure 6. XP spectra of the FBC sample. The sample spectrum is shown in black, with contributions to the sample spectra from Ce^{4+} shown in red and contributions from Ce^{3+} shown in blue.

4. DISCUSSION

Table 1. Ce^{3+} percentage values as determined by each technique on the commercial nanoceria materials.
*: Single calculation based on the fitting of a summation of multiple EEL spectra.

Sample	% Ce^{3+}, EELS*	% Ce^{3+}, XPS
NPCO	5.5	6.4 ± 0.9
FBC	35.2	<0.1

Ce^{3+} percentage values were determined from each technique for both samples and are listed in Table 1. Based on previous research suggesting that Ce^{3+} content increases

with decreasing particle size,[11] the FBC sample is expected to contain far more Ce^{3+} than the NPCO sample. The Ce^{3+} values for the NPCO sample as determined by the analytical techniques are in strong agreement (5.5% and ~6.5% for EELS and XPS, respectively). However, values for the FBC sample are quite different between the two techniques (~35% and <0.1% for EELS and XPS, respectively). Given the strong agreement of the two techniques for the NPCO sample (and to previous literature trends), this discrepancy is almost surely sample dependent. The FBC sample is comprised of nanoceria suspended in an aliphatic hydrocarbon solvent for its use as a diesel fuel additive. Given the small particle sizes in the FBC sample (and their metal oxide composition), they are expected to have very high surface energies and thus be poorly suspendable in various media. To overcome this, the nanoceria in the FBC are coated by a carbon-based surfactant to keep them suspended. This carbonaceous material was clearly seen in both the XPS C 1s spectrum (data not shown) and interacted with the electron beam during STEM imaging of the FBC sample (data not shown). It is possible that this carbon "contamination" compromised the oxidation state analysis of the FBC sample via XPS. Experiments are underway to determine how to overcome this issue.

5. CONCLUSION

In summary, we demonstrate the use of multiple analytical techniques for the orthogonal characterization of commercially available nanoceria materials using technique-independent controls. While EELS and XPS analyses were in strong agreement for the NPCO sample, the two techniques gave very conflicting results for the FBC sample. It is believed that this discrepancy was an artifact owing to the unique nature of the sample (heavily coated by a carbonaceous material). These results further highlight the importance of thorough characterization of experimental samples using orthogonal approaches due to the potential for differences to arise both from the analytical method chosen *and* the inherent properties of the analyte.

REFERENCES

1. Sun, C. W.; Li, H.; Chen, L. Q., Nanostructured ceria-based materials: synthesis, properties, and applications. *Energy & Environmental Science* **2012,** *5* (9), 8475-8505.
2. Xu, C.; Qu, X., Cerium oxide nanoparticle: a remarkably versatile rare earth nanomaterial for biological applications. *NPG Asia Mater* **2014,** *6*, e90.
3. Baalousha, M.; Ju-Nam, Y.; Cole, P. A.; Hriljac, J. A.; Jones, I. P.; Tyler, C. R.; Stone, V.; Fernandes, T. F.; Jepson, M. A.; Lead, J. R., Characterization of cerium oxide nanoparticles-part 2: nonsize measurements. *Environ Toxicol Chem* **2012,** *31* (5), 994-1003.
4. Spadaro, M. C.; D'Addato, S.; Gasperi, G.; Benedetti, F.; Luches, P.; Grillo, V.; Bertoni, G.; Valeri, S., Morphology, structural properties and reducibility of size-selected CeO2- x nanoparticle films. *Beilstein J Nanotechnol* **2015,** *6*, 60-7.
5. Spadaro, M. C.; Luches, P.; Bertoni, G.; Grillo, V.; Turner, S.; Tendeloo, G. V.; Valeri, S.; D'Addato, S., Influence of defect distribution on the reducibility of CeO 2− x nanoparticles. *Nanotechnology* **2016,** *27* (42), 425705.
6. Sims, C. M.; Maier, R. A.; Johnston-Peck, A. C.; Gorham, J. M.; Hackley, V. A.; Nelson, B. C. *Manuscipt in preparation.*
7. Fu, W. T.; Ijdo, D. J. W., The structure of CeAlO3 by Rietveld refinement of X-ray powder diffraction data. *Journal of Solid State Chemistry* **2004,** *177* (9), 2973-2976.
8. Verbeeck, J.; Van Aert, S., Model based quantification of EELS spectra. *Ultramicroscopy* **2004,** *101* (2–4), 207-224.
9. Barron, S. C.; Gorham, J. M.; Patel, M. P.; Green, M. L., High-Throughput Measurements of Thermochromic Behavior in V1–xNbxO2 Combinatorial Thin Film Libraries. *ACS Combinatorial Science* **2014,** *16* (10), 526-534.
10. Salvi, A. M.; Decker, F.; Varsano, F.; Speranza, G., Use of XPS for the study of cerium–vanadium (electrochromic) mixed oxides. *Surface and Interface Analysis* **2001,** *31* (4), 255-264.
11. Deshpande, S.; Patil, S.; Kuchibhatla, S. V. N. T.; Seal, S., Size dependency variation in lattice parameter and valency states in nanocrystalline cerium oxide. *Applied Physics Letters* **2005,** *87* (13), 133113.